frontiers in Materials

ORIGINAL RESEARCH
published: 04 June 2021
doi: 10.3389/fmats.2021.679682

Influence of Pre-Oxidation on High Temperature Oxidation and Corrosion Behavior of Ni-Based Aluminide Coating in Na_2SO_4 Salt at 1050°C

Qing Li[1], Defeng Zhang[2], Peng Song[1], Zhenhua Li[1], Ruixiong Zhai[1], Chen Hua[1] and Jiansheng Lu[1]*

[1]Faculty of Materials Science and Engineering, Kunming University of Science and Technology, Kunming, China, [2]School of Automotive Engineering, Yancheng Institute of Technology, Yancheng, China

Aluminide coating is prepared on K438 Ni-based superalloy by pack cementation. The hot corrosion test of as-received and pre-oxidation aluminide coating in Na_2SO_4 salt are carried out at 1050°C. The coating morphologies, phase composition, and corrosion products are characterized by XRD, SEM, EDS, and TEM. The conclusion is that the pre-oxidation aluminide coating has excellent hot corrosion properties. After hot corrosion, the oxide scale of pre-oxidation aluminide coating is the thinnest and maintains good integrity. However, the oxide scale of as-received aluminide coating fluctuates greatly and there are corrosion cavities. CrS is formed in the alloy immediately below the oxide scale for the two coating systems.

Keywords: hot corrosion, coating, alloy, TEM, oxide scale, alumina

OPEN ACCESS

Edited by:
Xin Zhou,
Wuhan University of Technology, China

Reviewed by:
Junbin Sun,
Hengyang Normal University, China
Xiaofeng Zhao,
Shanghai Jiao Tong University, China

****Correspondence:***
Peng Song
songpeng@kust.edu.cn

Specialty section:
This article was submitted to Ceramics and Glass, a section of the journal Frontiers in Materials

Received: *12 March 2021*
Accepted: *14 May 2021*
Published: *04 June 2021*

Citation:
Li Q, Zhang D, Song P, Li Z, Zhai R, Hua C and Lu J (2021) Influence of Pre-Oxidation on High Temperature Oxidation and Corrosion Behavior of Ni-Based Aluminide Coating in Na_2SO_4 Salt at 1050°C. Front. Mater. 8:679682. doi: 10.3389/fmats.2021.679682

INTRODUCTION

Ni-based superalloy has excellent creep resistance, high rupture strength, and corrosion resistance, so it is a perfect material for key components of aeroengines (He et al., 2015; Sun et al., 2015). They must be subjected to high temperature oxidation and hot corrosion by O_2 or other corrosive substances, for example, sulfur (Kosieniak et al., 2012; Yang et al., 2020). In heavy air pollution or coastal working environment, the metallic sulfates, such as Na_2SO_4, will be deposited on the surface of key components and accelerate their degradation (Eliaz et al., 2002; Wang et al., 2011). But the high temperature oxidation resistance of Ni-based superalloy is not good due to insufficient supply of Cr and Al at high temperature, which shortens the working life of blades. With the Cr or Al elements' depletion, the oxidation rate is accelerated and voids begin to form in the oxide scale, which provides a channel for the invasion of external corrosion particles (Liu et al., 2015; Yuan et al., 2015; Liu et al., 2016b). Therefore, it is necessary to apply protective coating on the surface of Ni-based superalloy to improve its high temperature properties.

The aluminide coating is usually used as the protective coating of Ni-based superalloy (Li et al., 2020). Aluminide coating has the following advantages: i) low cost and easy processing; ii) continuous, adhesive, and slow-growing oxide scale can be formed at a high temperature; and iii) excellent oxidation properties (Hou and Priimak, 2005; Hou and McCarty, 2006). Due to the rising engine-inlet temperature, the protective coatings have to be able to serve in a more aggressive environment because the aluminide coating is easy to generate void, crack, and spallation during long-term servicing. The high temperature oxidation and corrosion resistance of aluminide coating can be enhanced by adding many elements (Montero et al., 2013; Zhao and Zhou, 2014; Yang et al.,

TABLE 1 | Chemical composition (in wt. %)of K438 Ni-based superalloy.

Ni	C	Cr	Co	Al	Ti	W	Mo	Ta	Nb
Base	0.1~0.2	15.7~16.3	8.0~9.0	3.2~3.7	3.0~3.5	2.4~2.8	1.5~2.0	1.5~2.0	0.6~1.1

2016; Huang et al., 2020). The common methods for preparing aluminide coating are thermal spray, pack cementation, chemical vapor deposition, and hot-dipping (Hu et al., 2006; Zhang et al., 2012; Cheng et al., 2013; Shirvani et al., 2013; Xu et al., 2015; Sitek et al., 2016). Comparatively, the pack cementation process is simple and the cost is low, so it is suitable for specimens with higher requirements for bonding strength of the coating (Yuwen and Zhou, 2016; Yu et al., 2019).

Moreover, previous studies have found that the alloy is oxidized to form an excellent and dense oxide scale after pre-oxidation treatment, which hinders the oxidation and corrosion of alloy during the working, and the preparation and implementation are relatively simple (Matsumoto et al., 2006; Bao et al., 2008). The pre-oxidation treatment is beneficial to improve the oxidation and corrosion resistance of materials. Chen et al. (2008) studied the property of TBC pre-oxidation treatment. The results showed that α-Al_2O_3 film could be quickly formed on the bonding coating after TBC pre-oxidation treatment, which improves the high temperature oxidation properties and thermal cycle life of TBCs. Liu et al. (2010) found that the pre-oxidation scale can effectively reduce the corrosion rate of DZ68 alloy. The corrosion rate increases with the destruction of oxide scale, and the corrosion product fall off obviously.

Therefore, the pre-oxidation aluminide coating is prepared combined with the advantages of pre-oxidation. In addition, there are few studies on hot corrosion at the same pre-oxidation and corrosion temperature. In the study, the hot corrosion test is carried out by coating with Na_2SO_4 salt only once at 1050°C. The high temperature oxidation and corrosion behavior of aluminide coating in Na_2SO_4 salt is investigated by corrosion kinetics, cross-sectional microstructure, and composition distribution. Besides, the degradation of aluminide coating under this corrosion condition is discussed.

EXPERIMENTAL

Specimen Preparation

K438 Ni-based superalloy has good high temperature oxidation and corrosion resistance (Yu et al., 2019). The chemical constituents are listed in **Table 1**. The specimens of 17 mm diameter and 3 mm thickness were cut by wire. The specimens' surface was polished with 1,000-mesh sandpaper, then ultrasonically washed in anhydrous ethanol for 15 min and dried. By the equation of pack cementation mixed powder, 2Al - $4NH_4Cl$ - xSi - (94-x)Al_2O_3, the composition of mixed powder was 76.0 wt.% Al_2O_3, 20.4 wt.% AlSi40, and 3.6 wt.% NH_4Cl. The appropriate powder was weighed by balance and mixed evenly with a glass rod. Then the specimens were embedded in mixed powder, and then the crucible is placed in a tube furnace and heat-treated in Ar gas at 1000°C for 10 h until a stable aluminide coating was transformed. Then the specimen surface was polished with 1,000-mesh sandpaper until the surface of specimens showed a metallic luster. Then some specimens were pre-oxidized in a muffle furnace at 1050°C for 1 h. The residual specimens were as-received.

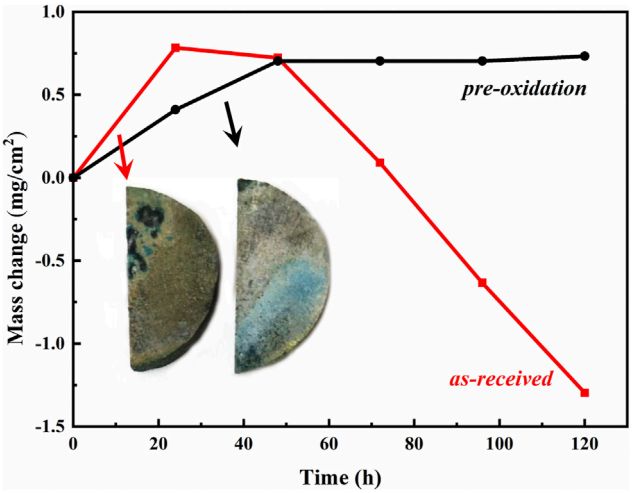

FIGURE 1 | mass change curves of aluminide coating during hot corrosion test in Na_2SO_4 salt at 1050°C.

Hot Corrosion Tests

The hot corrosion test was implemented by salt coating method at 1050°C. The specimens were preheated and coated with saturated Na_2SO_4 solution. The average amount of salt coating was 0.5–1.0 mg/cm^2. The above salt-coated specimens were put into a muffle furnace for hot corrosion test. The specimens were taken out for static cooling for 24 h as a cycle, weighing and observing the macroscopic morphology. Then five cycles were carried out in static air at 1050°C until the test time reached 120 h.

The analytical balance with precision of 0.1 mg was used during the test. The relationship between the mass change of specimens and corrosion time was recorded, and the corrosion kinetics curve was drawn. The surface and cross-sectional morphology of coating was observed and analyzed before and after corrosion by using a scanning electron microscope (SEM, FEI Quanta 6427) with energy dispersive spectrometer (EDS, Oxford INCA X-sight 6427), and the phase of coating was analyzed by using an X-ray diffractometer (XRD, BRUKER D8 Advance) with Cu Kα radiation (λ = 0.15405 nm) in the range 2θ = 20–90° with a step size of 0.02° and a counting time of 1 s per

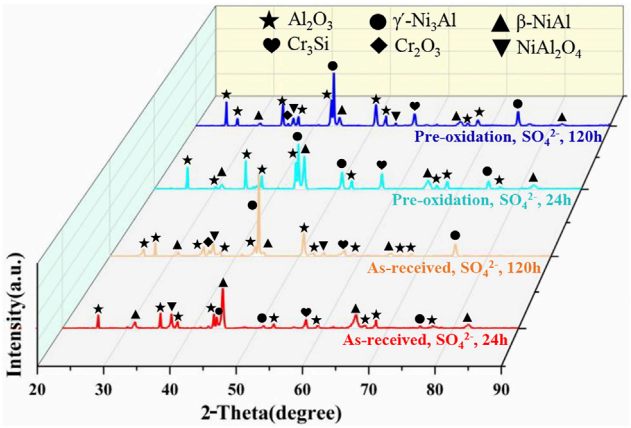

FIGURE 2 | XRD results of aluminide coating after hot corrosion for different time in Na_2SO_4 salt at 1050°C.

step to investigate the phase composition in the outermost layer of coating. The oxide scale was researched by using a transmission electron microscope (TEM, Tecnai G2 TF30), and the microstructure of oxide scale was determined. TEM specimens were prepared by focused ion beam (FIB).

RESULTS

Figure 1 shows the oxidation kinetics curve of as-received and pre-oxidation aluminide coating in Na_2SO_4 salt at 1050°C. The oxide scale formation leads to the mass change and the mass loss caused by oxide scale exfoliation or dissolution are obtained, and the corresponding conclusions are given in the experiment. During the first 24 h, the mass of as-received aluminide coating increased rapidly due to the growth of oxide scale. After 48 h of hot corrosion, the mass of as-received aluminide coating decreased rapidly, indicating that the oxide scale peeled off or dissolved. Obviously, the pre-oxidation aluminide coating has excellent corrosion properties, and the specimens' mass increases slowly and steadily after 48 h.

Figure 2 shows XRD results of the specimens after hot corrosion in Na_2SO_4 salt at 1050°C for 24 h and 120 h, respectively. The position and intensity of X-ray diffraction pattern can be found obviously. The presence of main phases on the coating surface of Al_2O_3, β-NiAl, γ'-Ni_3Al, Cr_3Si, and Cr_2O_3 is further confirmed using XRD, and $NiAl_2O_4$ phase peaks are observed. After 24 h, the corrosion product generated on two types of coatings chiefly composed of Al_2O_3. For two types of coatings, the peaks of γ'-Ni_3Al phase can be observed after hot corrosion for 120 h, indicating the consumption of aluminum in the coating leads to phase transformation of β-NiAl to γ'-Ni_3Al phase during hot corrosion test. And the oxide scale with poor protection containing Al_2O_3 and $NiAl_2O_4$ spinel phase is formed on two types of coatings. The $NiAl_2O_4$ spinel phase can be found on both coatings, but the peak intensity of $NiAl_2O_4$ phase on pre-oxidation aluminide coating is weaker than on as-received aluminide coating.

Figure 3 shows the surface topography of as-received and pre-oxidation aluminide coating on K438 superalloy in Na_2SO_4 salt at 1050°C after 120 h. **Figures 3C–F** are the local area of **Figures 3A,B** in high magnification, respectively. The surface morphology illustrated that serious oxide spallation is found above the as-received aluminide coating after hot corrosion covered by Na_2SO_4. In **Figure 3C**, corrosion cavities in the oxide scale can be observed by the magnifying image. After hot corrosion covered by Na_2SO_4 as shown in **Figures 3D,F**, there are two morphologies of Al_2O_3 on the pre-oxidation aluminide coating surface: nodule-shaped and needle-shaped. It means that there are still metastable oxides. The oxide scale spallation of pre-oxidation aluminide coating is less compared to as-received aluminide coating.

Figure 4 shows the cross-sectional microstructure of as-received and pre-oxidation aluminide coating after hot corrosion in Na_2SO_4 salt at 1050°C for 120 h. Apparently, the oxide scale of as-received aluminide coating is thicker than pre-oxidation aluminide coating, which is consistent with the mass change curve shown in **Figure 1**. Voids and cracks are found in the oxide scale of as-received aluminide coating after hot corrosion as shown in **Figure 4C**. The oxide scale of as-received aluminide coating has great fluctuation, indicating that the oxide grows inward during dissolution. The EDS results are shown in **Table 2**; points 1 and 2 in **Figure 4A** are obtained to be γ'-Ni3Al and β-NiAl in this order. On the contrary, the oxide scale formed by the pre-oxidation aluminide coating is the thinnest and maintains good integrity.

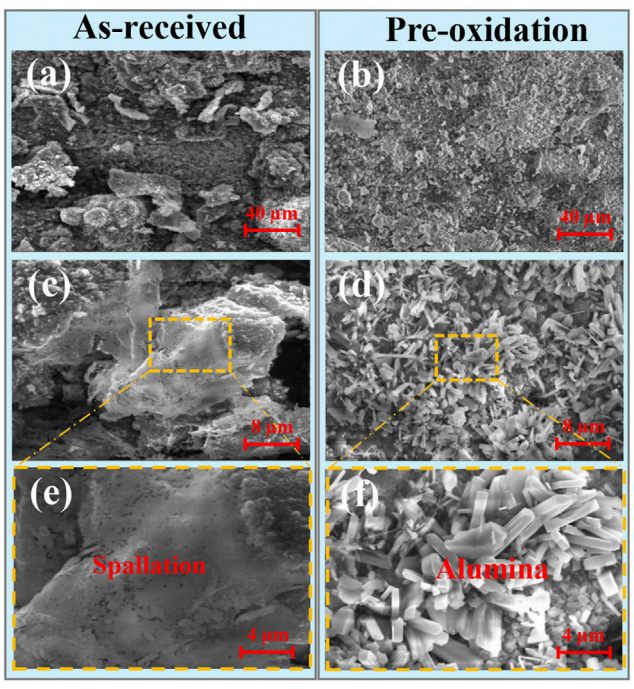

FIGURE 3 | Surface morphologies of the aluminide coating after hot corrosion for 120 h in Na_2SO_4 salt at 1050°C for **(A,C,E)** as-received and **(B,D,F)** pre-oxidation.

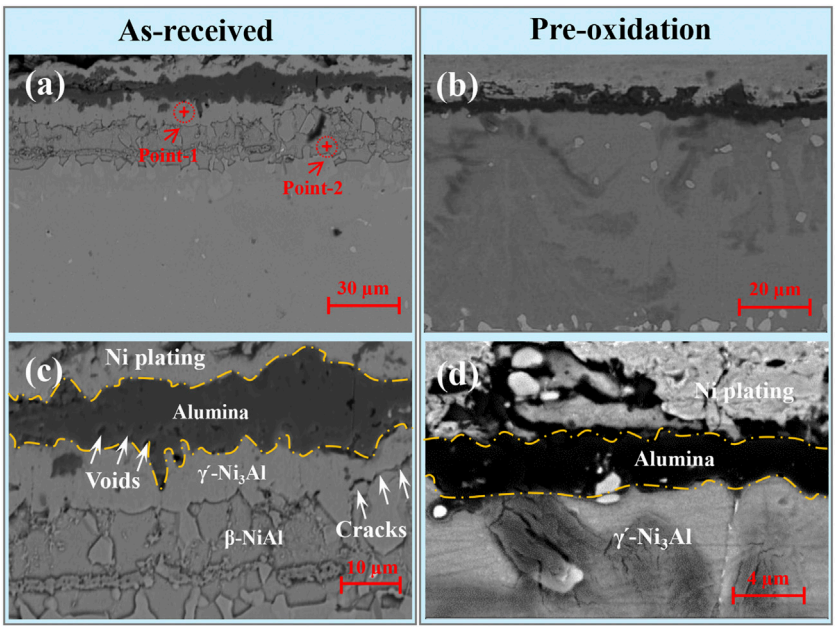

FIGURE 4 | Cross-sectional microstructures of the aluminide coating after hot corrosion for 120 h in Na_2SO_4 salt at 1050°C for **(A,C)** as-received and **(B,D)** pre-oxidation.

TABLE 2 | The chemical compositions (in at. %) of points in **Figure 4** by EDS.

Point	Ni	Co	Cr	O	Al	Si
1	66.1	8.2	5.1	0	19.2	1.4
2	44.1	7.2	9.9	4.1	34.5	0.2

Furthermore, in order to obtain the layer distribution information and mapping distribution image of corrosion specimens accurately, the line scanning and mapping scanning analysis methods of EDS are used. **Figure 5** shows that Al and O are mainly distributed on the surface of specimens, while the distribution of Cr is not uniform and there are some isolated regions rich in Cr. Similarly, from the line scan in **Figure 6** and **Figure 7**, there is signal S in the nickel-based alloy, indicating that the substrate has been sulfurized. The signal of S and Cr is consistent, indicating the formation of CrS.

DISCUSSION

During the initial stage of hot corrosion, electrons transfer from metal atoms to the reducing substances in the deposit, and the aluminide coating begins to be oxidized. The equation is as follows

$$\frac{4}{3}Al + O_2(g) = \frac{2}{3}Al_2O_3 \quad (1)$$

The initial reducing substances come from Na_2SO_4 and oxygen in the gaseous environment in **Figure 8**. The oxidation rate of aluminum on the coating surface is accelerated at the initial stage due to the increase of oxygen partial pressure. Then oxidation products are formed on the coating surface under the deposited salt, which is similar to the products obtained by the gas-coating reaction when there is no deposited salt on the surface of specimens. However, since sulfur also enters the specimens from the deposited salt, the difference still exists.

According to the corrosion kinetics curve, microstructure evolution, and element distribution, the pre-oxidation aluminide coating exhibits excellent hot corrosion resistance in Na_2SO_4 salt. The above results show that the oxide scale formed by pre-oxidation treatment can properly protect the specimens eroded by molten salt. The hot corrosion performance of pre-oxidation specimens in Na_2SO_4 salt at 1050°C for 120 h is obviously better than as-received specimens, and there is still a continuous pre-oxidation layer on the surface of specimens after hot corrosion. Meanwhile, even if sulfur exists in the high temperature environment, the oxide scale still has high stability. It may be due to the preformed continuous protective α-Al_2O_3, and the protective α-Al_2O_3 availably reduces the inward diffusion of sulfur. Therefore, the oxide scale slows the sulfuration of specimens and improves the oxidation property of specimens.

In general, there are two ways to be invaded by molten salt at the oxide-coating interface. First, the surface of specimens is completely coated with molten salt before the complete oxide scale is formed because the formation of continuous alumina takes time. The molten salts would spread and the specimens are invaded during the initial stage of hot corrosion. Thus, the oxide scale formed by pre-oxidation treatment can effectively prevent molten salt entering the specimens directly. So, the oxide-coating interface is comparatively smooth. The second method of molten salt invading oxide-coating interface is to generate cracks and voids in the oxide scale. The growth and dissolution of oxides occur at the same time during the hot corrosion process. The mass gain of pre-oxidation specimens in the first 24 h is smaller than as-received specimens, indicating that it

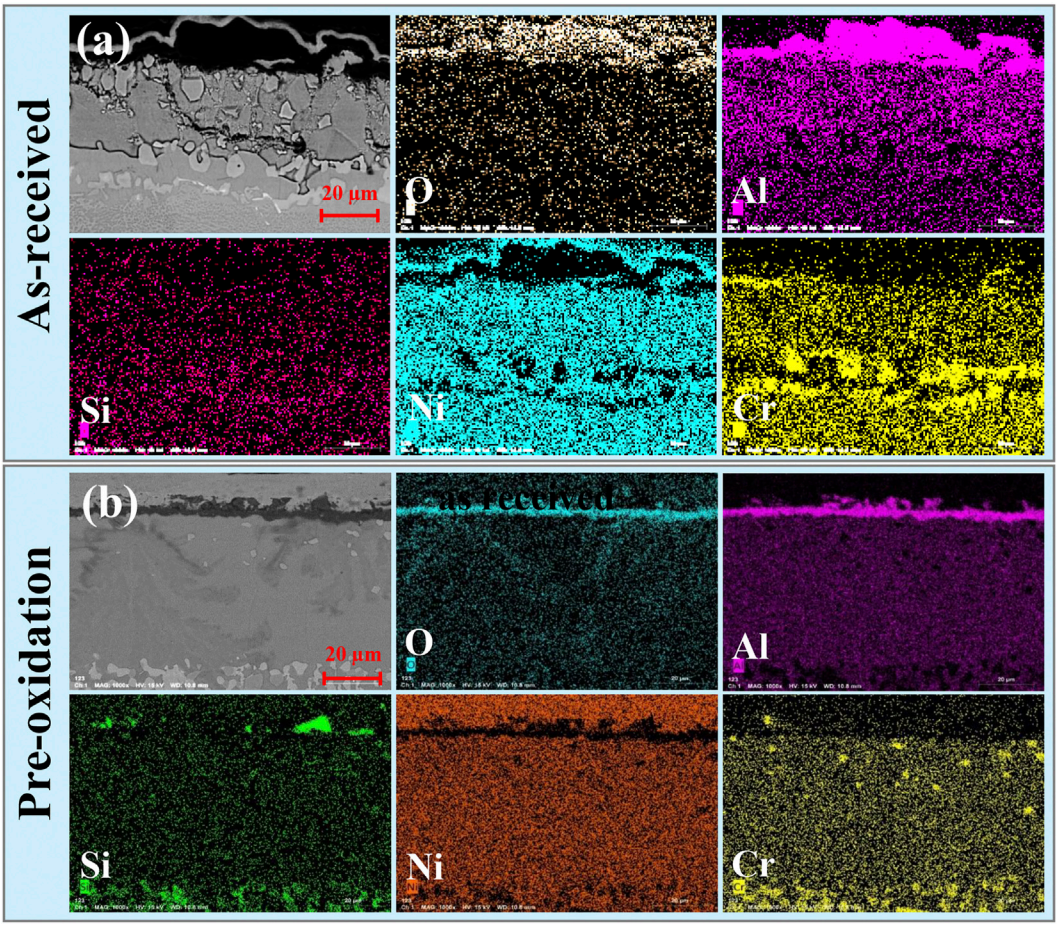

FIGURE 5 | EDS mapping of the aluminide coating cross section after hot corrosion for 120 h in Na_2SO_4 salt at 1050°C for **(A)** as-received and **(B)** pre-oxidation.

takes a long time to form a complete Al_2O_3 scale. As a result, the molten salts remain on the surface of coating. The molten salts would further promote the serious dissolution of oxide scale, resulting in a jagged morphology (see **Figures 4A,B**).

Due to the reaction between Na_2SO_4 and specimens, it is important that the sediments become alkaline or acidic than the original deposited state, and the thermodynamically stable phase diagram is shown in **Figure 9**. The change in the composition of these sediments affects the corrosion products' layer. When the deposited salt passes through the corrosion products' layer and comes in contact with the specimens, the degradation process would accelerate corrosion. As shown in **Figure 9**, the composition of Na_2SO_4 (melting point is 884°C in air) is determined by the oxygen partial pressure and the activity of Na_2O or SO_3 in the molten salt, according to the reaction

$$Na_2SO_4 = SO_3(g) + Na_2O \tag{2}$$

The alkaline melting occurs when the oxygen ion in the molten salt reacts with oxides to form solute. Bornstein and DeCrescente studies showed that hot corrosion can be caused by alkaline melting (Bornstein et al., 1973; Bornstein et al., 1989). During hot corrosion, the protective oxide scale is dissolved because of the reaction between Al_2O_3 scale and molten salt (Liu et al., 2016a; Yuwen and Zhou, 2016). The following reactions occur

$$Al_2O_3 + Na_2O = 2NaAlO_2 \tag{3}$$

$$2AlO_2^- = Al_2O_3 + O^{2-} \tag{4}$$

$$Ni^{2+} + 2AlO_2^- = NiAl_2O_4 \tag{5}$$

The interaction between outward diffusion of Ni^{2+} and inward diffusion AlO_2^- encountered and reacted with each other to form the $NiAl_2O_4$ (reaction **Eq. 5**). Therefore, XRD analysis shows the existence of $NiAl_2O_4$ spinel (**Figure 2**). Corrosion cavities can be clearly observed by the cross-sectional TEM morphology of oxide scale (**Figure 10A**). There are three morphologies of corrosion cavities as shown in **Figure 10B**. The corrosion cavities can be divided into the following three stages: nucleation (occurrence), expansion (development), and deep cavity (result). Therefore, the possible causes of corrosion cavities in the oxide scale can be reasonably inferred. The reaction **Eq. 3** forms AlO_2^- concentration gradient in the oxide scale. According to the fluxing mechanism, AlO_2^- forms at the metal/scale interface and moves outward in the molten salts, and then converts to porous Al_2O_3 particles where the oxygen partial pressure is high, as the **Eq. 4** in the article.

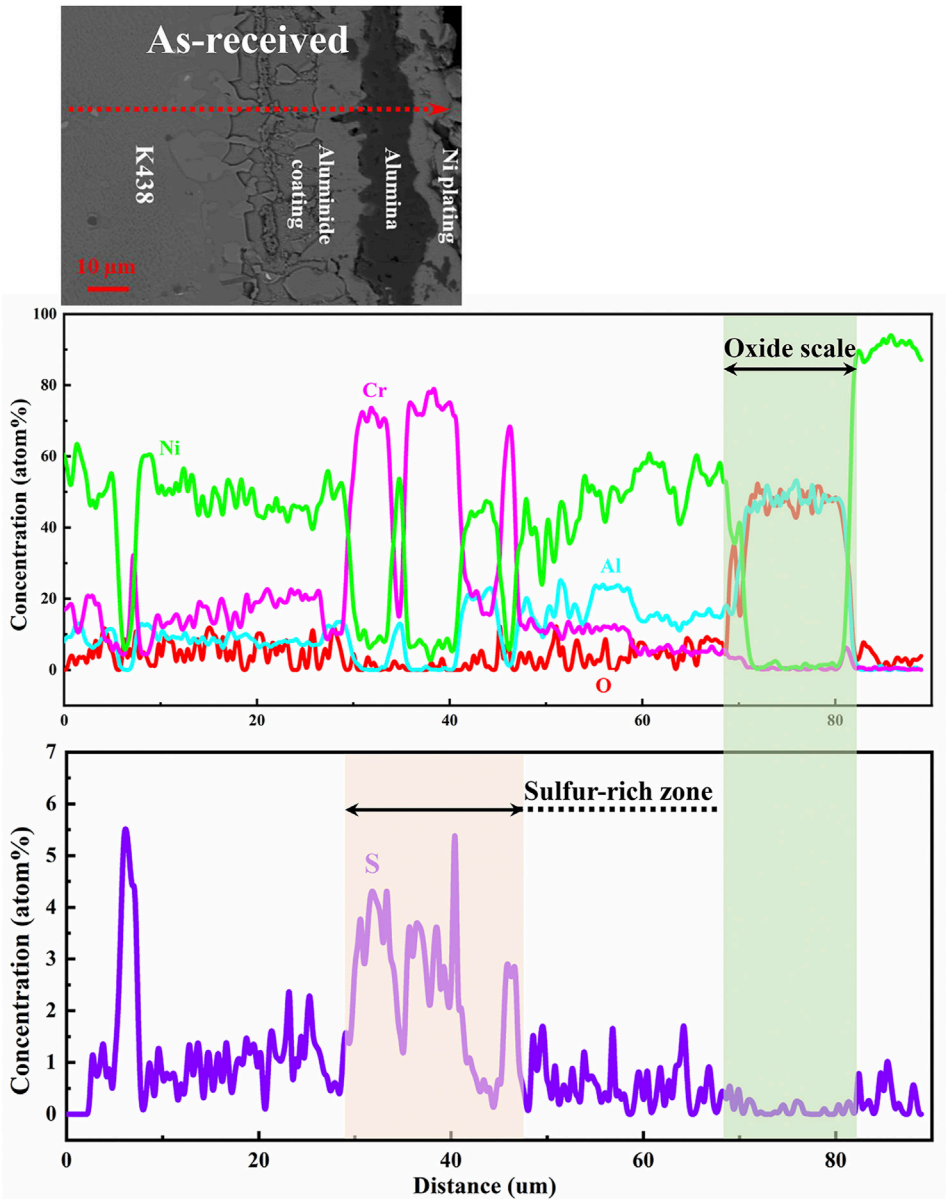

FIGURE 6 | Line scan of the as-received aluminide coating cross section after hot corrosion for 120 h in Na_2SO_4 salt at 1050°C.

Shores and Mohanty (2004) found that the deposited salt is distributed in the corrosion cavities of oxide scale in most cases, and the surface tension effect plays an important role in the distribution of deposited salt. It is reasonable to assume that the deposited salt on the surface of specimens is a continuous film at the early stage of hot corrosion. However, the salt is more likely to be distributed in the corrosion cavities of unprotected oxides at the hot corrosion expanding stage. The corrosion may be uneven on the whole surface of specimens. As shown in **Figure 6** and **Figure 7**, CrS is formed in the alloy immediately below the oxide scale. Upon coating with Na_2SO_4 salt at 1050°C, the reaction of producing S_2 is as follows (Yuan and Wang, 2010)

$$2SO_4^{2-} = 2O^{2-} + 3O_2(g) + S_2(g) \tag{6}$$

The released S_2 reacts with the substrate to form CrS. The affinity of Cr-S is stronger than Ni-S (Li et al., 2006). The reaction is as follows

$$2Cr + S_2(g) = 2CrS \tag{7}$$

$$\frac{4}{3}Cr + O_2(g) = \frac{2}{3}Cr_2O_3 \tag{8}$$

The results show that Cr_2O_3 at the oxide scale is more likely formed by direct oxidation of Cr. It strongly proves the reason for Cr_2O_3 occurrence in the oxide scale, as shown in **Figure 2**.

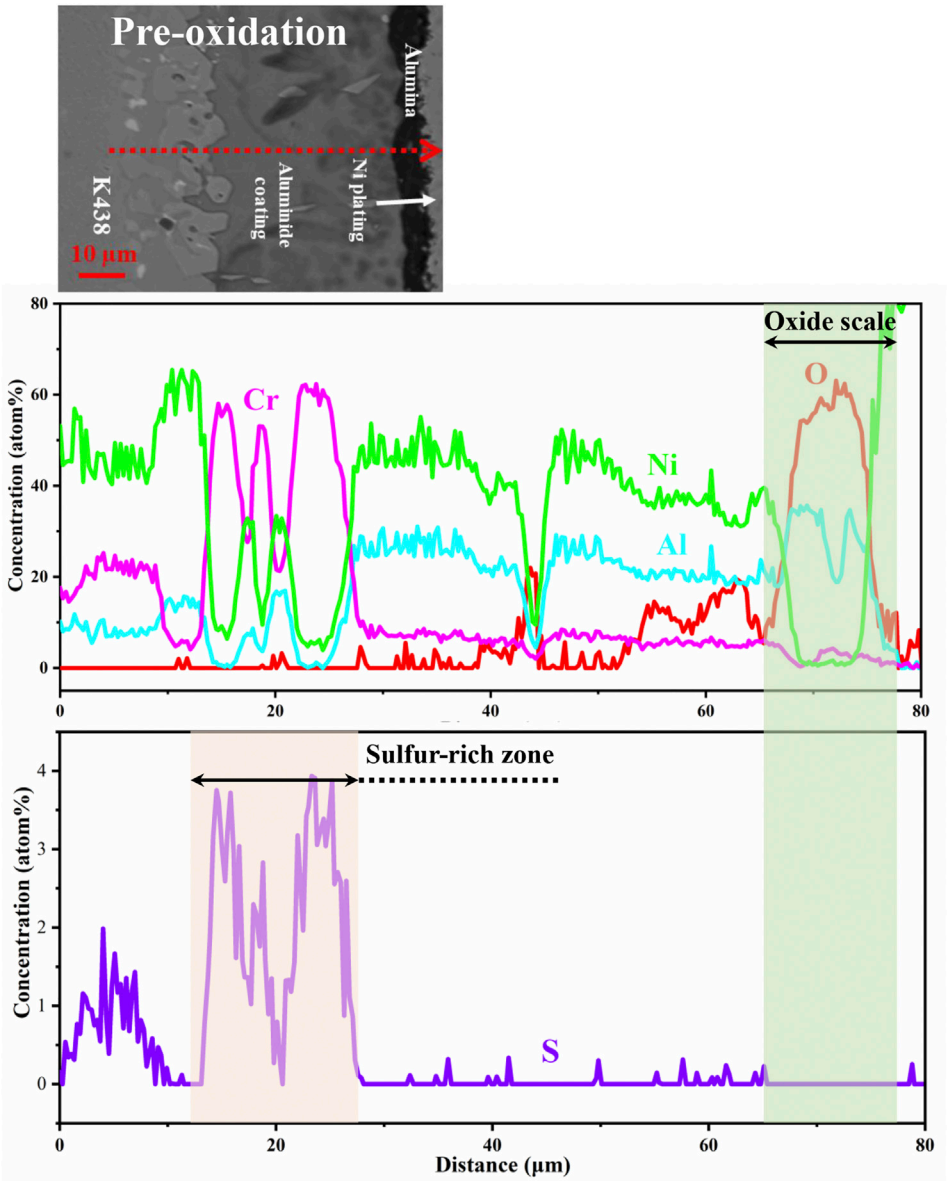

FIGURE 7 | Line scan of the pre-oxidation aluminide coating cross section after hot corrosion for 120 h in Na_2SO_4 salt at 1050°C.

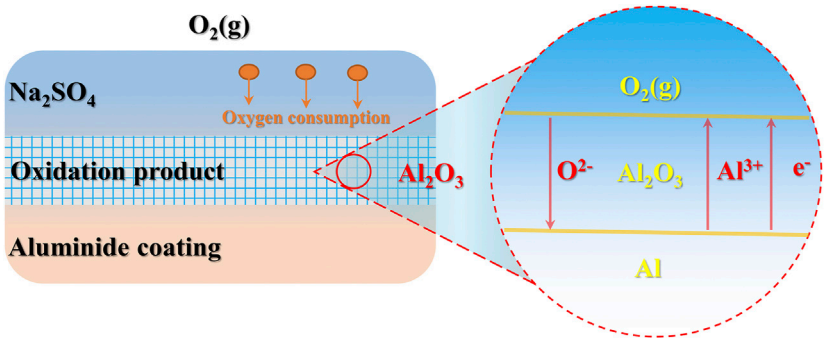

FIGURE 8 | Schematic diagram of aluminide coating oxygen consumption during the initial stage of hot corrosion.

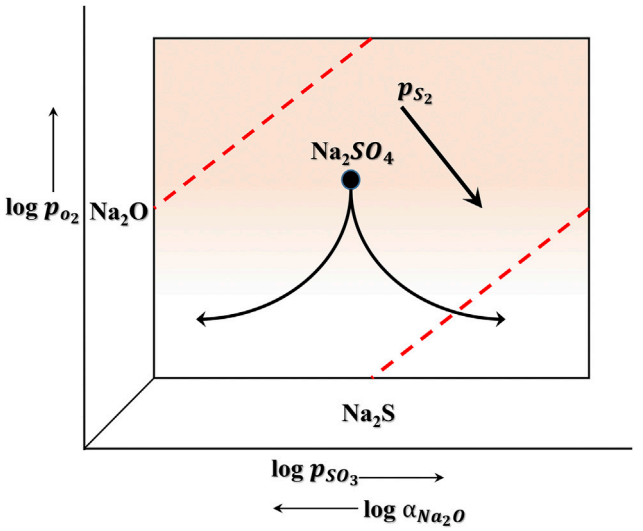

FIGURE 9 | Thermodynamically stable phase diagram of Na-O-S system at constant temperature.

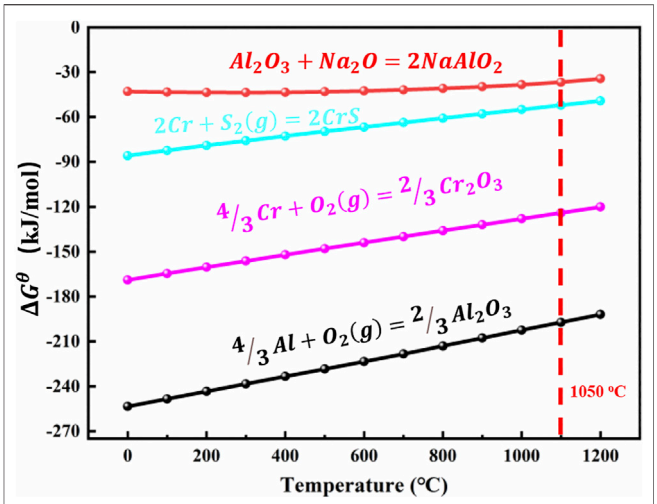

FIGURE 11 | Standard Gibbs free energy changes (ΔGθ) of forming compounds as a function of temperature.

There are complex chemical reactions during hot corrosion. The main causes of hot corrosion are explored by calculating the thermodynamic Gibbs free energy of each reaction. The standard Gibbs free energy reaction is $\Delta G_T^\theta = \Delta H_{298}^\theta + \int_{298}^{\theta} \Delta C_p dT - T\Delta S_{298}^\theta - T\int_{298}^{\theta} \Delta C_p dlnT$; it is related to the initial state and final state of reaction. In the experiment, the ΔG_T^θ values of various chemical reactions at 1050°C are analyzed by using HSC Chemistry 6.0 software, as shown in **Figure 11**. The ΔG_T^θ value of chemical reactions is negative, so these reactions occur spontaneously. **Figure 12** shows the schematic diagram of two coatings' hot corrosion process to describe clearly the coating degradation process. The alkaline melting described above has several obvious characteristics, which are as follows: i) due to the release of sulfur from Na_2SO_4, sulfides are found in the alloy and ii) the corrosion degree depends on the oxygen ions' amount formed in salt.

CONCLUSION

The aim of present work is to investigate the high temperature oxidation and corrosion behavior of Ni-based aluminide coating in Na_2SO_4 salt. The following conclusions can be drawn from the above study:

(1) The mass change curve of two coating systems indicates that the pre-oxidation aluminide coating has excellent hot corrosion properties. The mass of as-received aluminide coating decreases rapidly, but the pre-oxidation aluminide coating mass increases slowly and steadily after 48 h.

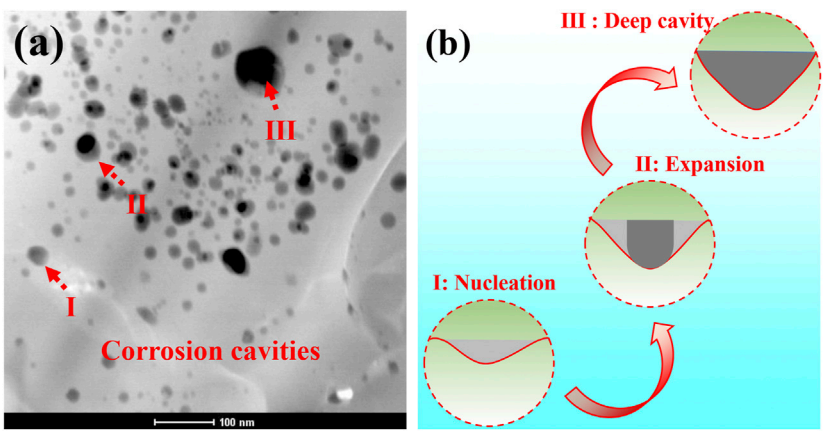

FIGURE 10 | (A) Cross-sectional TEM morphology of oxide scale formed on the as-received aluminide coating after hot corrosion for 120 h in Na_2SO_4 salt at 1050°C; **(B)** the schematic diagram of corrosion cavity morphology.

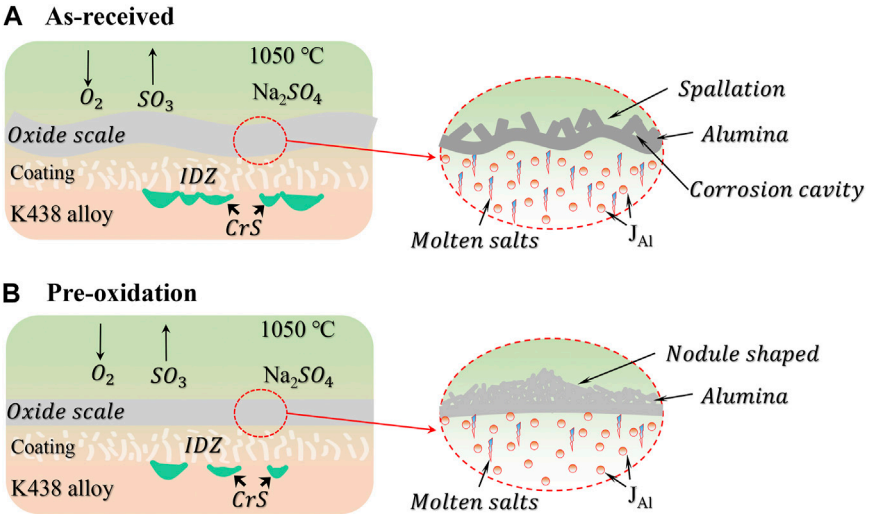

FIGURE 12 | A schematic illustration of corrosion mechanism of aluminide coating for **(A)** as-received and **(B)** pre-oxidation.

(2) After hot corrosion, the oxide scale of pre-oxidation aluminide coating is the thinnest and maintains good integrity. But the oxide scale of as-received aluminide coating has great fluctuation, indicating that the oxide grows inward during dissolution.
(3) CrS is formed in the alloy immediately below the oxide scale due to the affinity of Cr-S being stronger than Ni-S.
(4) As corrosion cavities are observed in the oxide scale of as-received aluminide coating, the salt is more likely to be distributed in the corrosion cavities of unprotected oxides during hot corrosion.

DATA AVAILABILITY STATEMENT

The original contributions presented in the study are included in the article/Supplementary Material; further inquiries can be directed to the corresponding author.

AUTHOR CONTRIBUTIONS

QL: conceptualization, methodology, investigation, writing-original draft, and data curation. PS: funding acquisition, data curation, validation, writing - review and editing, and supervision. DZ, ZL: writing-review and editing, and supervision. RZ, CH: experiment and data curation. JL: conceptualization and supervision.

FUNDING

This work was financially supported by the National Natural Science Foundation of China (No. 52071168), the Yunnan Province Science Technology Major Project (No. 2019ZE001), the Rare and Precious Metal Materials Genome Engineering Project of Yunnan Province (No. 202002AB080001).

REFERENCES

Bao, Z. B., Wang, Q. M., Li, W. Z., Gong, J., Xiong, T. Y., and Sun, C. (2008). Corrosion Behaviour of AIP NiCoCrAlYSiB Coating in Salt spray Tests. *Corrosion Sci.* 50 (3), 847–855. doi:10.1016/j.corsci.2007.09.004

Bornstein, N. S., DeCrescente, M. A., and Roth, H. A. (1973). The Relationship between Relative Oxide Ion Content of Na2SO4, the Presence of Liquid Metal Oxides and Sulfidation Attack. *Metall. Trans.* 4 (8), 1799–1810. doi:10.1007/bf02665406

Bornstein, N. S., DeCrescente, M. A., and Smeggil, J. G. (1989). The Influence of Sulfur on the Oxidation of Coatings. *Mater. Sci. Eng. A.* 120-121, 175–178. doi:10.1016/0921-5093(89)90736-3

Chen, W. R., Wu, X., Marple, B. R., Lima, R. S., and Patnaik, P. C. (2008). Pre-oxidation and TGO Growth Behaviour of an Air-Plasma-Sprayed thermal Barrier Coating. *Surf. Coat. Technology* 202 (16), 3787–3796. doi:10.1016/j.surfcoat.2008.01.021

Cheng, W.-J., Liao, Y.-J., and Wang, C.-J. (2013). Effect of Nickel Pre-plating on High-Temperature Oxidation Behavior of Hot-Dipped Aluminide Mild Steel. *Mater. characterization* 82, 58–65. doi:10.1016/j.matchar.2013.05.007

Eliaz, N., Shemesh, G., and Latanision, R. M. (2002). Hot Corrosion in Gas Turbine Components. *Eng. Fail. Anal.* 9 (1), 31–43. doi:10.1016/s1350-6307(00)00035-2

He, H., Liu, Z., Wang, W., and Zhou, C. (2015). Microstructure and Hot Corrosion Behavior of Co-si Modified Aluminide Coating on Nickel Based Superalloys. *Corrosion Sci.* 100, 466–473. doi:10.1016/j.corsci.2015.08.011

Hou, P. Y., and McCarty, K. F. (2006). Surface and Interface Segregation in β-NiAl with and without Pt Addition. *Scripta materialia*. 54 (5), 937–941. doi:10.1016/j.scriptamat.2005.10.065

Hou, P. Y., and Priimak, K. (2005). Interfacial Segregation, Pore Formation, and Scale Adhesion on NiAl Alloys. *Oxid Met.* 63 (1), 113–130. doi:10.1007/s11085-005-1954-3

Hu, T. L., Huang, H. L., Gan, D., and Lee, T. Y. (2006). The Microstructure of Aluminized Type 310 Stainless Steel. *Surf. Coat. Technology* 201 (6), 3502–3509. doi:10.1016/j.surfcoat.2006.07.254

Huang, T., Lü, J., Song, P., Khan, A., Chen, R., and Yi, J. (2020). Effect of Pt Doping on Oxide Scale Formation on Yttria-Dispersion FeCrAl alloy at 1200℃. *Corrosion Sci.* 168, 108580. doi:10.1016/j.corsci.2020.108580

Kosieniak, E., Biesiada, K., Kaczorowski, J., and Innocenti, M. (2012). Corrosion Failures in Gas Turbine Hot Components. *J. Fail. Anal. Preven.* 12 (3), 330–337. doi:10.1007/s11668-012-9571-3

Li, C., Huang, T., Song, P., Yuan, X., Feng, J., Lü, K., et al. (2020). Effect of Water Vapour on Morphology of the Si/Ti-Rich Phase at the Interface between Oxide Layer and Aluminide Coating. *Corrosion Sci.* 163, 108240. doi:10.1016/j.corsci.2019.108240

Li, M., Sun, X., Hu, W., Guan, H., and Chen, S. (2006). Hot Corrosion of a Single Crystal Ni-Base Superalloy by Na-Salts at 900°C. *Oxid Met.* 65 (1), 137–150. doi:10.1007/s11085-006-9004-3

Liu, E., Zheng, Z., Guan, X., Tong, J., Ning, L., and Yu, Y. (2010). Influence of Pre-oxidation on the Hot Corrosion of DZ68 Superalloy in the Mixture of Na2SO4-NaCl. *J. Mater. Sci. Technology* 26 (10), 895–899. doi:10.1016/s1005-0302(10)60143-0

Liu, R. D., Jiang, S. M., Yu, H. J., Gong, J., and Sun, C. (2016a). Preparation and Hot Corrosion Behaviour of Pt Modified AlSiY Coating on a Ni-Based Superalloy. *Corrosion Sci.* 104, 162–172. doi:10.1016/j.corsci.2015.12.007

Liu, X., An, Y., Zhao, X., Li, S., Deng, W., Hou, G., et al. (2016b). Hot Corrosion Behavior of NiCoCrAlYTa Coating Deposited on Inconel alloy Substrate by High Velocity Oxy-Fuel Spraying upon Exposure to Molten V 2 O 5 -containing Salts. *Corrosion Sci.* 112, 696–709. doi:10.1016/j.corsci.2016.09.010

Liu, Z., Zhao, X., and Zhou, C. (2015). Improved Hot Corrosion Resistance of Y-Ce-Co-Modified Aluminide Coating on Nickel Base Superalloys by Pack Cementation Process. *Corrosion Sci.* 92, 148–154. doi:10.1016/j.corsci.2014.11.043

Matsumoto, M., Hayakawa, K., Kitaoka, S., Matsubara, H., Takayama, H., Kagiya, Y., et al. (2006). The Effect of Preoxidation Atmosphere on Oxidation Behavior and thermal Cycle Life of thermal Barrier Coatings. *Mater. Sci. Eng. A.* 441 (1-2), 119–125. doi:10.1016/j.msea.2006.08.099

Montero, X., Galetz, M. C., and Schütze, M. (2013). Sulphidation Behavior of a Non Harmful Water-Based Al and Al-Si Slurry Coating on CM247 Superalloy. *Oxid Met.* 80 (5), 635–649. doi:10.1007/s11085-013-9412-0

Shirvani, K., Mastali, S., Rashidghamat, A., and Abdollahpour, H. (2013). The Effect of Silicon on thermal Shock Performance of Aluminide-thermal Barrier Coatings. *Corrosion Sci.* 75, 142–147. doi:10.1016/j.corsci.2013.05.025

Shores, D. A., and Mohanty, B. P. (2004). Role of Chlorides in Hot Corrosion of a Cast Fe-Cr-Ni alloy. Part II: Thermochemical Model Studies. *Corrosion Sci.* 46 (12), 2909–2924. doi:10.1016/j.corsci.2004.04.014

Sitek, R., Bolek, T., Dobosz, R., Plocinski, T., and Mizera, J. (2016). Microstructure and Oxidation Resistance of Aluminide Layer Produced on Inconel 100 Nickel alloy by CVD Method. *Surf. Coat. Technology* 304, 584–591. doi:10.1016/j.surfcoat.2016.07.072

Sun, C., Kirk, M., Li, M., Hattar, K., Wang, Y., Anderoglu, O., et al. (2015). Microstructure, Chemistry and Mechanical Properties of Ni-Based Superalloy Rene N4 under Irradiation at Room Temperature. *Acta Materialia.* 95, 357–365. doi:10.1016/j.actamat.2015.04.061

Wang, Y., Suneson, M., and Sayre, G. (2011). Synthesis of Hf-Modified Aluminide Coatings on Ni-Base Superalloys. *Surf. Coat. Technology* 206 (6), 1218–1228. doi:10.1016/j.surfcoat.2011.08.031

Xu, Z., Dai, J., Niu, J., He, L., Mu, R., and Wang, Z. (2015). Isothermal Oxidation and Hot Corrosion Behaviors of Diffusion Aluminide Coatings Deposited by Chemical Vapor Deposition. *J. Alloys Compounds* 637, 343–349. doi:10.1016/j.jallcom.2015.01.227

Yang, Y. F., Jiang, C. Y., Yao, H. R., Bao, Z. B., Zhu, S. L., and Wang, F. H. (2016). Cyclic Oxidation and Rumpling Behaviour of Single Phase β-(Ni,Pt)Al Coatings with Different Thickness of Initial Pt Plating. *Corrosion Sci.* 111, 162–174. doi:10.1016/j.corsci.2016.05.011

Yang, Y. F., Liu, Z. L., Ren, P., Wang, Q. W., Bao, Z. B., Zhu, S. L., et al. (2020). Hot Corrosion Behavior of Pt+Hf Co-modified NiAl Coating in the Mixed Salt of Na2SO4-NaCl at 900 °C. *Corrosion Sci.* 167, 108527. doi:10.1016/j.corsci.2020.108527

Yu, X., Song, P., He, X., Khan, A., Huang, T., Li, C., et al. (2019). Influence of the Combined-Effect of NaCl and Na2SO4 on the Hot Corrosion Behaviour of Aluminide Coating on Ni-Based Alloys. *J. Alloys Compounds* 790, 228–239. doi:10.1016/j.jallcom.2019.03.165

Yuan, K., Lin Peng, R., Li, X.-H., Talus, A., Johansson, S., and Wang, Y.-D. (2015). Hot Corrosion of MCrAlY Coatings in Sulphate and SO 2 Environment at 900 °C: Is SO 2 Necessarily Bad?. *Surf. Coat. Technology* 261, 41–53. doi:10.1016/j.surfcoat.2014.11.065

Yuan, L., and Wang, H. (2010). Hot Corrosion Behaviors of a Cr13Ni5Si2-Based Metal Silicide alloy in Na_2SO_4+25wt.%K_2SO_4 and Na_2SO_4+25wt.% NaCl Molten Salts. *Intermetallics.* 18 (3), 324–329. doi:10.1016/j.intermet.2009.08.004

Yuwen, P., and Zhou, C. (2016). Improved Hot Corrosion Resistance of Dy-Co-Modified Aluminide Coating by Pack Cementation Process on Nickel Base Superalloys. *Corrosion Sci.* 112, 710–717. doi:10.1016/j.corsci.2016.09.011

Zhang, Z. G., Peng, Y. P., Mao, Y. L., Pang, C. J., and Lu, L. Y. (2012). Effect of Hot-Dip Aluminizing on the Oxidation Resistance of Ti-6Al-4V alloy at High Temperatures. *Corrosion Sci.* 55, 187–193. doi:10.1016/j.corsci.2011.10.029

Zhao, X., and Zhou, C. (2014). Effect of Y2O3 Content in the Pack on Microstructure and Hot Corrosion Resistance of Y-Co-Modified Aluminide Coating. *Corrosion Sci.* 86, 223–230. doi:10.1016/j.corsci.2014.05.018

Conflict of Interest: The authors declare that the research was conducted in the absence of any commercial or financial relationships that could be construed as a potential conflict of interest.